

Suppression of basal autophagy in neural cells causes neurodegenerative disease in mice

Taichi Hara¹, Kenji Nakamura², Makoto Matsui^{1,3,4}, Akitsugu Yamamoto⁵, Yohko Nakahara², Rika Suzuki-Migishima², Minesuke Yokoyama⁶, Kenji Mishima⁷, Ichiro Saito⁷, Hideyuki Okano^{8,9} & Noboru Mizushima^{1,10}

Autophagy is an intracellular bulk degradation process through which a portion of the cytoplasm is delivered to lysosomes to be degraded^{1–4}. Although the primary role of autophagy in many organisms is in adaptation to starvation, autophagy is also thought to be important for normal turnover of cytoplasmic contents, particularly in quiescent cells such as neurons. Autophagy may have a protective role against the development of a number of neurodegenerative diseases^{5–8}. Here we report that loss of autophagy causes neurodegeneration even in the absence of any disease-associated mutant proteins. Mice deficient for *Atg5* (autophagy-related 5) specifically in neural cells develop progressive deficits in motor function that are accompanied by the accumulation of cytoplasmic inclusion bodies in neurons. In *Atg5*^{-/-} cells, diffuse, abnormal intracellular proteins accumulate, and then form aggregates and inclusions. These results suggest that the continuous clearance of diffuse cytosolic proteins through basal autophagy is important for preventing the accumulation of abnormal proteins, which can disrupt neural function and ultimately lead to neurodegeneration.

Every eukaryotic cell has two main systems for the degradation of intracellular components: the ubiquitin–proteasome system and autophagy. Autophagy is a generic term for the degradation of cellular components in lysosomes^{1–4}. Macroautophagy (hereafter referred to as autophagy) is believed to be the main pathway among several subtypes of autophagy. During the process of autophagy, small portions of cytoplasm are sequestered by autophagosomes and then degraded on fusion with lysosomes. In contrast to the ubiquitin–proteasome system, which accounts for most of the selective intracellular protein degradation, autophagy is less selective. Autophagy induced by starvation is a mechanism for producing amino acids within cells. In yeast, autophagy-defective cells are susceptible to starvation. In comparison, mice deficient for *Atg5* and *Atg7*, which are essential for autophagosome formation⁹, suffer from severe nutrient- and energy-insufficiency soon after birth^{10,11}. Thus, adaptation to starvation is an evolutionarily conserved role of autophagy.

In addition to induced autophagy, a low level of constitutive autophagy is important for intracellular clearance under normal conditions. Mice bearing a liver-specific conditional knockout allele of *Atg7* show hepatic dysfunction and intracellular ubiquitin-positive inclusion bodies¹¹. We have also observed the accumulation of ubiquitin-positive inclusion bodies in hepatocytes and a subset of neurons in *Atg5*-knockout (*Atg5*^{-/-}) neonates (Supplementary

Fig. S1); however, conventional histological analysis revealed no significant abnormality¹⁰. These data suggest that intracellular protein quality-control by autophagy is particularly important in neural cells. Indeed, several studies have suggested that impairment of autophagy could worsen the accumulation of abnormal proteins in neurodegenerative disease models *in vitro* and *in vivo*^{5–8}. However, direct evidence demonstrating that autophagy contributes to the prevention of neurodegeneration has been lacking, in part because *Atg5*^{-/-} and *Atg7*^{-/-} mice die soon after birth^{10,11}.

To determine the role of autophagy in neural cells, we generated neural-cell-specific *Atg5*^{-/-} mice (Supplementary Fig. S2). Mice bearing an *Atg5*^{flox} allele, in which exon 3 of the *Atg5* gene is flanked by two *loxP* sequences, were crossed with a transgenic line expressing Cre recombinase under the control of the nestin promoter (*nestin-Cre*)¹². In these mice, Cre recombinase is expressed in neural precursor cells after embryonic day (E)10.5, causing deletion of the *loxP*-flanked exon 3 (Supplementary Fig. S3). Recombination was successful in over 90% of all brain cells from *Atg5*^{flox/flox}; *nestin-Cre* mice. The expression of *Atg5* (detected as an *Atg12*–*Atg5* conjugate¹³) and the *Atg5*-dependent conversion of microtubule-associated protein 1 light chain 3 (LC3)-I to LC3-II (LC3–phosphatidylethanolamine (LC3-PE) conjugate)^{13,14} were almost completely suppressed in the brains of *Atg5*^{flox/flox}; *nestin-Cre* mice after E15.5 (Fig. 1a and Supplementary Fig. S3). These data suggest that autophagosome formation is impaired in the brains of these mutant mice.

Atg5^{flox/flox}; *nestin-Cre* mice were born normally and survived neonatal starvation. They did not show the suckling defects observed in *Atg5*^{-/-} and *Atg7*^{-/-} neonates^{10,11}, suggesting that an undetectable, but sufficient, level of *Atg5* remains in the neurons controlling the suckling response at this stage, or that non-neural cells may mediate the suckling deficit in the non-conditional mutants. However, the *Atg5*^{flox/flox}; *nestin-Cre* mice showed growth retardation: their mean body weight was about 1.5-times lower than that of control (*Atg5*^{flox/+}; *nestin-Cre*) mice (Fig. 1b). *Atg5*^{flox/flox}; *nestin-Cre* mice developed progressive motor and behavioural deficits after three weeks of age, and footprint analysis revealed an ataxic walking pattern (Fig. 1c). Mean stride lengths corrected for paw base widths were significantly decreased compared with control (*Atg5*^{flox/+}; *nestin-Cre*) mice. The *Atg5*^{flox/flox}; *nestin-Cre* mice showed limb-clasping reflexes when they were suspended by their tails, whereas control mice extended their limbs (Fig. 1d). This abnormal reflex is often observed in mouse models of neurodegenerative disease^{15,16}.

¹Department of Bioregulation and Metabolism, Tokyo Metropolitan Institute of Medical Science, Tokyo 113-8613, Japan. ²Mouse Genome Technology Laboratory, Mitsubishi Kagaku Institute of Life Sciences, Tokyo 194-8511, Japan. ³Department of Basic Biology, School of Life Science, the Graduate University for Advanced Studies, Okazaki 444-8585, Japan. ⁴Department of Cell Biology, National Institute for Basic Biology, Okazaki 444-8585, Japan. ⁵Department of Bio-Science, Nagahama Institute of Bio-Science and Technology, Nagahama 526-0829, Japan. ⁶Brain Research Institute, Niigata University, Niigata 951-8510, Japan. ⁷Department of Pathology, Tsurumi University School of Dental Medicine, Yokohama 230-8501, Japan. ⁸Department of Physiology, Keio University School of Medicine, Tokyo 160-8582, Japan. ⁹SORST and ¹⁰PRESTO, Japan Science and Technology Agency, Kawaguchi 332-0012, Japan.

Rotarod (Fig. 1e) and wire-hanging (data not shown) tasks also showed severely impaired motor coordination, balance and grip strength in *Atg5^{flox/flox}; nestin-Cre* mice. Finally, tremor was apparent in 12-week-old mice. Some of the *Atg5^{flox/flox}; nestin-Cre* mice died after three weeks of age. Neither *Atg5^{flox/flox}* mice (Cre-negative) nor *Atg5^{flox/+}; nestin-Cre* mice showed any abnormal phenotype.

The gross anatomy of the brain of the mutant mice was normal. However, histological examination revealed degenerative changes in the neurons of *Atg5^{flox/flox}; nestin-Cre* mice. These alterations were most prominent in cerebellar Purkinje cells. Haematoxylin and eosin (H&E) staining (arrowheads in Fig. 2a) and immunohistochemical staining with an antibody directed against calbindin (a selective marker for Purkinje cells, left panels in Fig. 2b), demonstrated partial loss of these neurons (Fig. 2c). The remaining Purkinje cells showed eccentrically located nuclei, with infolding of the nuclear membrane. We also found a number of eosinophilic spheroids in H&E-stained sections in the cerebellar nuclei of these mutant mice (arrows in Fig. 2a), which probably correspond to the calbindin-positive spheroids in the same region (Fig. 2b, right panels). These structures suggest massive swelling of Purkinje cell axons that project to the cerebellar nuclei^{17,18}. In addition, TUNEL-positive cells were detected in the adjacent granular layer, suggesting apoptosis of granular cells in *Atg5^{flox/flox}; nestin-Cre* mice (Fig. 2d). Consistent with previous

observations, the survival of granular cells largely depends on their synaptic connectivity with Purkinje cells¹⁹. Axonal swelling was observed in other regions of the *Atg5^{flox/flox}; nestin-Cre* brain, including the cerebral cortex, the nucleus gracilis (Fig. 2a), the posterior thalamic nucleus, hippocampus, inferior colliculus, trigeminal nucleus, parabrachial nucleus, anterior thalamic nucleus, caudal pons and reticular nucleus (data not shown). Partial loss of pyramidal cells also was observed in the cerebral cortex (data not shown). Together, these data suggest that *Atg5^{flox/flox}; nestin-Cre* mice suffer from neurodegeneration.

We next examined protein aggregation in the brain using an antibody against ubiquitin, a marker of misfolded proteins. Large, ubiquitin-positive inclusion bodies accumulated in the cytoplasm of large neurons in the thalamus, pons, medulla, dorsal root ganglion (DRG) (Fig. 3a) and midbrain (data not shown) of *Atg5^{flox/flox}; nestin-Cre* mice. Neurons in the cerebral cortex, hippocampus (especially in the CA3 and CA4 regions) (Fig. 3a), striatum and olfactory bulb (data not shown) were also positive for these inclusion

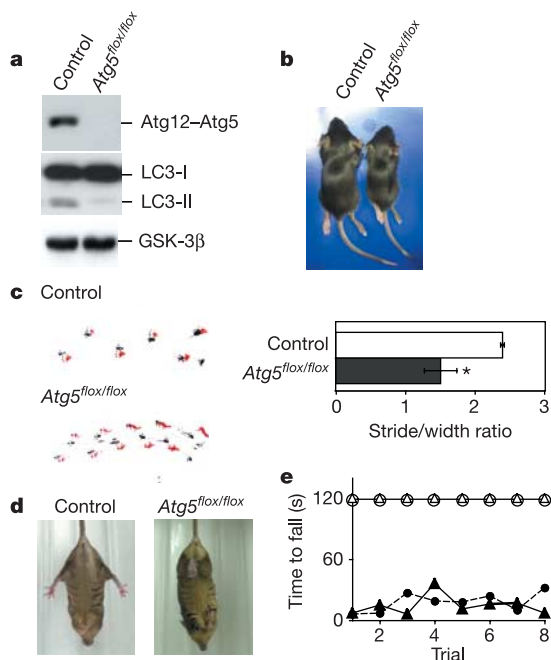


Figure 1 | Behavioural abnormalities in mice lacking Atg5 in the nervous system. **a**, Immunoblot analysis of Atg5 and LC3. Brain homogenates were prepared from six-week-old control (*Atg5^{flox/+}; nestin-Cre*) and *Atg5^{flox/flox}; nestin-Cre* (*Atg5^{flox/flox}*) mice. Immunoblot analysis was performed using antibodies against Atg5 and LC3. GSK-3 β was used as a loading control. The positions of the Atg12-Atg5 conjugate, LC3-I and LC3-II (LC3-PE conjugate) are indicated. Atg5 monomer was not detected in either lane (data not shown). **b**, A representative male control (*Atg5^{flox/+}; nestin-Cre*) and an *Atg5^{flox/flox}; nestin-Cre* (*Atg5^{flox/flox}*) littermate at three weeks of age. **c**, Left, paw placement records of eight-week-old mice. Right, stride lengths corrected for paw base widths (stride/width ratio) of *Atg5^{flox/flox}; nestin-Cre* and control (*Atg5^{flox/+}; nestin-Cre*) littermate mice. Values represent means \pm s.d. of four mice. Asterisk, $P < 0.01$ (Student's *t*-test). **d**, Abnormal limb-clasping of an *Atg5^{flox/flox}; nestin-Cre* mouse compared with a control mouse (*Atg5^{flox/+}; nestin-Cre*) when suspended by its tail. **e**, Rotarod testing of *Atg5^{flox/+}; nestin-Cre* (open symbols) and *Atg5^{flox/flox}; nestin-Cre* (closed symbols) mice. One male and one female mouse were analysed for each genotype. The time until drop from the rod (rotating at 20 r.p.m.) is shown.

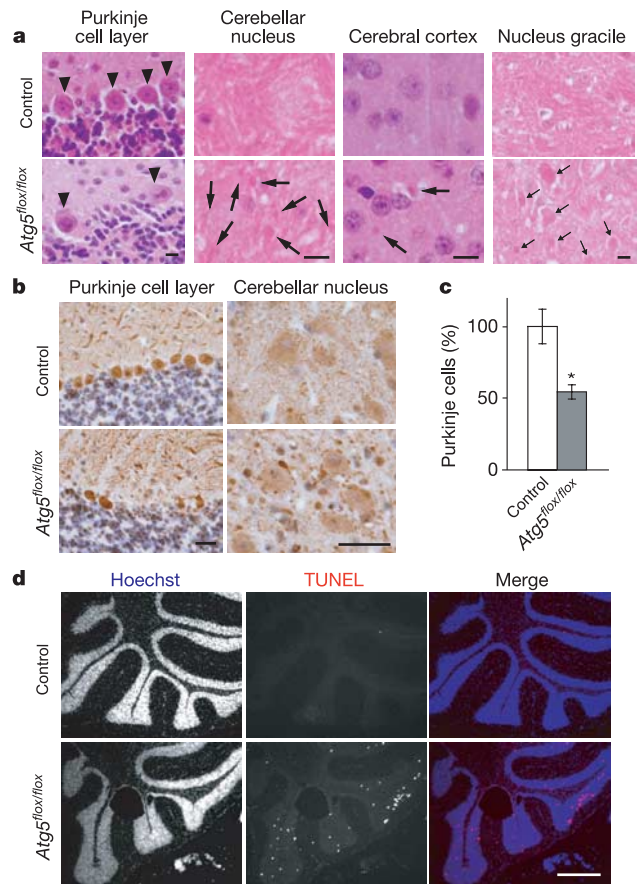


Figure 2 | Neuronal degeneration in *Atg5^{flox/flox}; nestin-Cre* mice. **a**, H&E-stained sections of the cerebral cortex, the gracile nucleus and cerebellum from control (*Atg5^{flox/+}; nestin-Cre*) and *Atg5^{flox/flox}; nestin-Cre* (*Atg5^{flox/flox}*) mice at three months of age. Purkinje cells are indicated with arrowheads. Arrows indicate eosinophilic spheroids, which represent axon swelling. Scale bar, 10 μ m. **b**, Immunohistochemistry using an anti-calbindin antibody on cerebellum sections from control (*Atg5^{flox/+}; nestin-Cre*) and *Atg5^{flox/flox}; nestin-Cre* mice at six weeks of age. Scale bar, 25 μ m. **c**, Loss of Purkinje cells in *Atg5^{flox/flox}; nestin-Cre* mice. Purkinje cells were counted in comparable areas for each mouse, and three fields were counted in each area for each mouse. Data are normalized against values from control mice (*Atg5^{flox/+}; nestin-Cre*). Values represent mean \pm s.d. of three mice. Asterisk, $P < 0.01$ (*t*-test). **d**, Apoptotic death of granular cells. Cerebellum sections from control (*Atg5^{flox/+}; nestin-Cre*) and *Atg5^{flox/flox}; nestin-Cre* mice at six weeks of age were subjected to TUNEL staining. Nuclei were stained with Hoechst 33258. Scale bar, 500 μ m.

bodies. Such inclusion bodies were not observed in the brains of control ($Atg5^{flox/+}$; *nestin-Cre*) mice. We observed ubiquitin-positive inclusion bodies exclusively in cells positive for the neural cell marker NeuN, suggesting that inclusion bodies were generated only in neurons and not in glial cells (Fig. 3b). Notably, although there was extensive loss of Purkinje cells, these neurons had very few inclusion bodies in their cell bodies (Fig. 3a). Numerous ubiquitin-positive dots were observed in the cerebellar nuclei (Fig. 3a), but most of them did not colocalize with the calbindin dots observed in Fig. 2b (data not shown).

The accumulation of inclusion bodies was time-dependent, and the distribution of inclusion-body-positive cells was more limited in $Atg5^{-/-}$ and $Atg5^{flox/flox}$; *nestin-Cre* newborns compared to adult mice. In $Atg5^{-/-}$ neonates, inclusion bodies were observed in the pons, DRG, spinal cord (ventral horn) (Supplementary Fig. S1), hypothalamus, midbrain and trigeminal ganglia (data not shown), but not in the cerebral cortex (Supplementary Fig. S1). A similar pattern was observed in the brain and DRG of $Atg5^{flox/flox}$; *nestin-Cre* neonates (Supplementary Fig. S4 and data not shown). Immunoelectron microscopy of DRG neurons isolated from $Atg5^{-/-}$ neonates

demonstrated the specific association of ubiquitin with amorphous, occasionally filamentous, structures (Fig. 3c, left), as well as with more compact structures surrounded by filamentous materials (Fig. 3c, right; see Supplementary Fig. S5 for larger images). Outside the brain, $Atg5^{-/-}$ neonates showed inclusion body formation in the liver, the anterior lobe of pituitary gland (Supplementary Fig. S1) and the adrenal gland (data not shown).

Histological examination of $Atg5^{-/-}$ and $Atg5^{flox/flox}$; *nestin-Cre* mice suggested that, in addition to the presence of inclusion bodies, the intensity of diffuse cytoplasmic ubiquitin staining was higher compared with wild-type mice. We thus analysed the time course of accumulation of diffuse ubiquitinated proteins and inclusions in DRG neurons (the neonatal tissue in which inclusion body formation was most striking). DRG neurons from $Atg5^{-/-}$ embryos at E13.5 had no apparent abnormality. However, at E15.5, some neurons had accumulated diffuse, cytosolic ubiquitinated proteins with infrequent inclusions (Fig. 4a). Later, in newborn (postnatal day (P)0) $Atg5^{-/-}$ mice, multiple ubiquitin-positive inclusion bodies were present in DRG neurons. Thus, the accumulation of diffuse abnormal proteins seems to be the primary cellular phenotype of $Atg5^{flox/flox}$; *nestin-Cre* neurons. We obtained similar results using a biochemical method with whole brains. Polyubiquitinated proteins that accumulated in $Atg5^{flox/flox}$; *nestin-Cre* brains were primarily Triton-soluble in six-week-old mice (Fig. 4b). In contrast, in 14-week-old mice, Triton-insoluble polyubiquitinated proteins were also abundant, suggesting that inclusion body formation is a later event.

We confirmed these observations using hepatocytes, another cell type that showed extensive inclusion body accumulation under autophagy-defective conditions¹¹ (Supplementary Fig. S1). We crossed $Atg5^{flox/flox}$ mice with CAG-*Cre* mice that express Cre recombinase ubiquitously (see Methods)²⁰. As recombination efficiency was not high when crossed with our $Atg5^{flox/flox}$ mice, the resulting mice ($Atg5^{flox/flox}$; CAG-*Cre*) were mosaic for the mutant allele and viable. In the livers of these mice, the *Atg5* gene was deleted in only about 30% of hepatocytes (Supplementary Fig. S6), which allowed us to compare directly the immunoreactivity of knockout cells with that of wild-type cells in the same specimen. Anti-ubiquitin staining of the liver in four-month-old $Atg5^{flox/flox}$; CAG-*Cre* mice showed that about 30% of cells had very high levels of diffuse cytoplasmic signals (in addition to inclusion bodies), compared with surrounding cells that were probably wild type (Fig. 4c). The results clearly demonstrate that cytosolic ubiquitinated proteins also accumulate in $Atg5^{-/-}$ hepatocytes.

We then determined the time course of accumulation of ubiquitinated proteins using Mx1-*Cre* transgenic mice²¹. In this system, Cre recombinase is expressed under the control of an interferon-responsive promoter that can be activated by application of polyinosinic acid-polycytidylic acid (pIpC), an interferon-inducible, synthetic double-stranded RNA. The *Atg5* gene in $Atg5^{flox/flox}$; Mx1-*Cre* liver was deleted by intraperitoneal injection of pIpC. Soon after injection, most targeted cells showed only diffuse ubiquitin staining, with no inclusion bodies (Fig. 4d, e). In contrast, large, ubiquitin-positive inclusion bodies were present in almost all targeted hepatocytes 16 days after pIpC injection (arrowheads in Fig. 4d). Cells with only inclusion bodies but not diffuse cytoplasmic staining were observed very rarely. Taken together, our data demonstrate that loss of autophagy first leads to accumulation of diffuse abnormal proteins, followed by generation of inclusion bodies.

We have shown that the inhibition of autophagy in neural cells causes neurodegeneration and symptoms of neurological pathology. As the mouse model we used does not express any disease-associated mutant proteins, the phenotype of these mutant mice indicates that autophagy mediates essential and continuous turnover of intracellular proteins. This system is particularly important for neurons, in which deregulation of this degradation process can induce cell dysfunction. The role of autophagy could be even more critical if

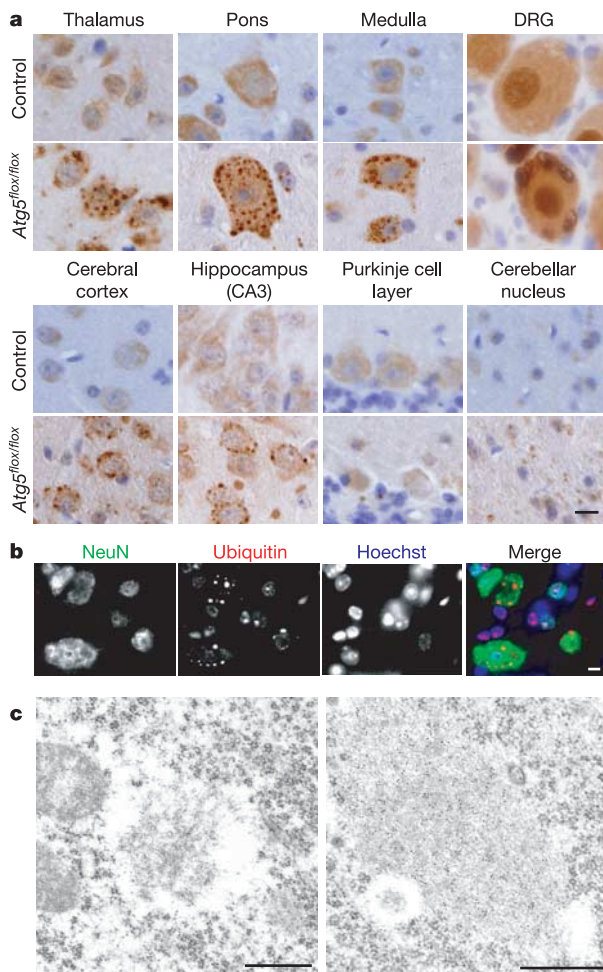


Figure 3 | Ubiquitin-positive inclusions in *Atg5*-deficient neurons. **a**, Immunohistochemistry of brain sections from control ($Atg5^{flox/+}$; *nestin-Cre*) and $Atg5^{flox/flox}$; *nestin-Cre* ($Atg5^{flox/flox}$) mice at six weeks of age, stained with an anti-ubiquitin antibody (1B3). Scale bar, 10 μ m. **b**, Ubiquitin-positive inclusions in neurons. Sections of medulla from $Atg5^{flox/flox}$; *nestin-Cre* mice at six weeks of age were stained with an antibody against NeuN (a neuron-specific nuclear protein) and ubiquitin. Nuclei were stained with Hoechst 33258. Scale bar, 10 μ m. **c**, Immunoelectron microscopy of ubiquitin-positive inclusion bodies. DRG neurons isolated from $Atg5^{-/-}$ neonates were analysed by immunoelectron microscopy using an anti-ubiquitin antibody. Scale bars, 500 nm.

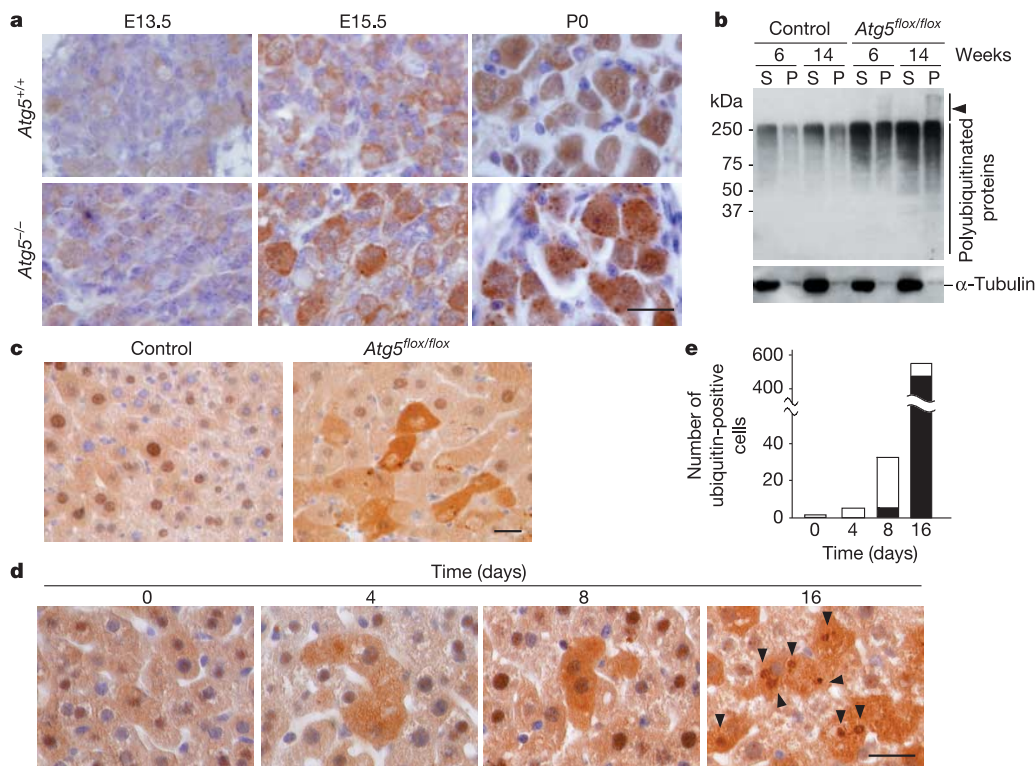


Figure 4 | Accumulation of diffuse ubiquitinated proteins in autophagy-defective cells. **a**, Immunohistochemistry of DRG neurons from *Atg5*^{+/+} and *Atg5*^{-/-} mice at different developmental stages (embryonic day (E)13.5, E15.5 or postnatal day (P)0), stained with an antibody directed against ubiquitin. Scale bar, 25 μ m. **b**, Accumulation of Triton-X-100-soluble polyubiquitinated proteins in the brains of *Atg5*^{flox/flox}; *nestin-Cre* mice. Brain homogenate prepared at the indicated times from control (*Atg5*^{flox/+}; *nestin-Cre*) and *Atg5*^{flox/flox}; *nestin-Cre* (*Atg5*^{flox/flox}) mice were separated into Triton-X-100-soluble (S) and -insoluble (P) fractions and analysed by immunoblotting using anti-ubiquitin antibodies. Arrowhead indicates the

stacking gel. **c**, Immunohistochemistry of liver sections from control (*Atg5*^{flox/+}; *CAG-Cre*) and *Atg5*^{flox/flox}; *CAG-Cre* (*Atg5*^{flox/flox}) mice at four months of age, using an anti-ubiquitin antibody. Scale bar, 25 μ m. **d**, Immunohistochemistry of liver sections from six-week-old *Atg5*^{flox/flox}; *Mx1-Cre* mice at the indicated time points after pIpC injection, using anti-ubiquitin antibodies. Arrowheads indicate ubiquitin-positive inclusion bodies. Scale bar, 25 μ m. **e**, Five thousand hepatocytes were randomly selected, and the number of cells with diffuse cytosolic ubiquitin signals, with (black) or without (white) inclusion bodies, were counted.

any aggregation-prone mutant proteins were expressed. Although autophagy is generally thought to be a non-selective process, several studies have suggested that autophagosomes can specifically engulf inclusion bodies^{8,22}. In our system, however, inclusion bodies appeared in later phases of autophagy deficiency, suggesting that the primary role of autophagy under normal conditions is the turnover of diffuse cytosolic proteins, not direct elimination of inclusion bodies. As the population of ubiquitinated proteins in *Atg5*^{flox/flox}; *nestin-Cre* brains was similar to that in wild-type mouse brains, we suggest that cytoplasmic proteins that are usually ubiquitinated, rather than specific proteins, accumulate in larger amounts in the absence of autophagy (Supplementary Fig. S7). Downregulation of protein turnover could cause the accumulation of abnormal proteins, which then could promote aggregate formation (Supplementary Fig. S8).

The critical role of autophagy in the basal turnover of diffuse cytosolic proteins in neural cells should be emphasized, because it has been suggested that large inclusion bodies themselves might not be pathogenic, but that mutant proteins present diffusely in the cytosol could be the primary source of toxicity^{23–27}. However, we do not rule out the possibility that autophagosomes can selectively recognize abnormal soluble proteins or microaggregates on the membrane surface. It was recently reported that the polyubiquitin-binding protein p62/SQSTM1 might mediate the specific recognition of protein aggregates by autophagosomes²⁸. This pathway might also be involved in the degradation of diffuse ubiquitinated proteins by autophagy.

METHODS

Generation of tissue-specific *Atg5*-deficient mice. An approximately 1-kb *Xba*I–*Spe*I mouse genomic fragment containing putative exon 3 of the *Atg5* gene was flanked by two *loxP* sites containing the neomycin-resistant (*neo*^r) cassette from pMC1-Neo (Stratagene). The diphtheria toxin A (*DT-A*) gene was inserted downstream of the short arm, for negative selection against random integration of the vector (Supplementary Fig. S2). Targeted CCE embryonic stem cells of 129/SvEv mouse origin were injected into C57BL/6 blastocysts, and chimaeric mice were crossed with C57BL/6 mice to obtain *Atg5*^{flox/+} mice. We used the following primers to detect wild-type *Atg5* and *Atg5*^{flox} alleles: A (exon3-1), 5'-GAATATGAAGGCACACCCCTGAAATG-3'; B (short2), 5'-GTACTGCATAATGGTTAACTCTTGC-3'; C (check2), 5'-ACAACGTCGAGCACAGCTGCGCAAGG-3'; D (5L2), 5'-CAGGAATGGTGTCTCCAC-3'; E (cre1), 5'-AGGTTCGTTCACTCATGGA-3'; F (cre2), 5'-TCGACCAGTTT AGTACCC-3'.

Southern blot analysis was performed using the probe shown in Supplementary Fig. S2 after digestion of genomic DNA with *Eco*RV and *Kpn*I, as described previously¹³. *Nestin-Cre* transgenic mice expressing Cre recombinase under the control of the mouse *nestin* gene promoter and second intronic neural enhancer (a gift from S. Noguchi) have been described previously²⁹. *CAG-Cre* transgenic mice expressing Cre recombinase under the control of the *CAG* (CMV enhancer and chicken β -actin) promoter have been described previously²⁰. *Mx1-Cre* transgenic mice were obtained from the Jackson Laboratory²¹. Progeny containing the *Atg5*^{flox} allele were bred with these Cre transgenic mice to generate *Atg5*^{flox/flox}; *nestin-Cre*, *Atg5*^{flox/flox}; *CAG-Cre* and *Atg5*^{flox/flox}; *Mx1-Cre* mice. *Atg5*^{-/-} mice have been described previously¹⁰. All animal experiments were approved by the institutional committee of the Tokyo Metropolitan Institute of Medical Science.

Antibodies. A monoclonal antibody against ubiquitin (1B3) was purchased from

MBL and used for immunohistochemistry. Rabbit anti-ubiquitin polyclonal antibody (DakoCytomation) was used for immunoelectron microscopy. Anti-polyubiquitin monoclonal antibody (FK2, Nippon Bio-Test Laboratories) was used in immunoblot analyses. The following antibodies were also used: anti-NeuN monoclonal antibody (Chemicon), rabbit anti-calbindin polyclonal antibody (Chemicon), Alexa Fluor 488- and 660-conjugated goat anti-rabbit IgG (H + L) antibodies (Molecular Probes), monoclonal anti-glycogen synthase kinase-3 β antibody (BD Biosciences), monoclonal anti- α -tubulin antibody (DM1A, Sigma-Aldrich), and antibodies against Atg5 (SO4)¹³ and LC3¹⁴.

Behavioural analysis. Mice were placed on a rod rotating at 20 r.p.m., and the time taken for them to fall from the rod was measured. If a mouse stayed on the rod until the end of the 2-min trial, a time of 120 s was recorded.

Immunohistochemical analysis. Mice were transcardially perfused with 4% paraformaldehyde in phosphate buffer (pH 7.4). Tissues were post-fixed in the same fixative overnight and embedded in paraffin. Sections were stained using Meyer's H&E. For immunohistochemical analysis, all tissue sections were subjected to antigen retrieval using the microwave method (in 0.01 M citrate buffer for 10 min). After blocking, sections were incubated with primary antibodies for 1 h, followed by 30 min incubation with fluorescently labelled or biotinylated secondary antibodies that were detected using Histomouse-plus kits (Zymed Laboratories) and the Liquid DAB substrate chromogen system (DakoCytomation). Apoptotic cells were detected by TUNEL assay using an *in situ* cell death detection kit (Roche Diagnostic).

Immunoelectron microscopy. For immunoelectron microscopy, the post-embedding immuno-gold method was used to label tissue sections embedded with LR white resin (London Resin Co.) as previously described³⁰.

Preparation of detergent-soluble and -insoluble fractions. Mouse brains were homogenized in five volumes of ice-cold 0.25 M sucrose buffer (50 mM Tris-HCl pH 7.4, 1 mM EDTA) with protease inhibitors. Homogenates were centrifuged at 500g for 10 min at 4 °C, and the resulting supernatants were lysed with an equal volume of cold sucrose buffer containing 1% Triton X-100. Lysates were subjected to centrifugation at 13,000g for 15 min at 4 °C to separate supernatants (fractions soluble in 0.5% Triton-X-100) and pellets. Pellets were resuspended in 1% SDS in PBS (Triton-X-100-insoluble fractions).

Received 6 February; accepted 20 March 2006.

Published online 19 April 2006.

- Cuervo, A. M. Autophagy: in sickness and in health. *Trends Cell Biol.* **14**, 70–77 (2004).
- Levine, B. & Klionsky, D. J. Development by self-digestion: molecular mechanisms and biological functions of autophagy. *Dev. Cell* **6**, 463–477 (2004).
- Klionsky, D. J. The molecular machinery of autophagy: unanswered questions. *J. Cell Sci.* **118**, 7–18 (2005).
- Mizushima, N. The pleiotropic role of autophagy: from protein metabolism to bactericide. *Cell Death Differ.* **12**, 1535–1541 (2005).
- Ravikumar, B., Duden, R. & Rubinsztein, D. C. Aggregate-prone proteins with polyglutamine and polyalanine expansions are degraded by autophagy. *Hum. Mol. Genet.* **11**, 1107–1117 (2002).
- Fortun, J., Dunn, W. A. Jr, Joy, S., Li, J. & Notterpek, L. Emerging role for autophagy in the removal of aggregates in Schwann cells. *J. Neurosci.* **23**, 10672–10680 (2003).
- Ravikumar, B. *et al.* Inhibition of mTOR induces autophagy and reduces toxicity of polyglutamine expansions in fly and mouse models of Huntington disease. *Nature Genet.* **36**, 585–595 (2004).
- Iwata, A. *et al.* Increased susceptibility of cytoplasmic over nuclear polyglutamine aggregates to autophagic degradation. *Proc. Natl Acad. Sci. USA* **102**, 13135–13140 (2005).
- Mizushima, N., Ohsumi, Y. & Yoshimori, T. Autophagosome formation in mammalian cells. *Cell Struct. Funct.* **27**, 421–429 (2002).
- Kuma, A. *et al.* The role of autophagy during the early neonatal starvation period. *Nature* **432**, 1032–1036 (2004).
- Komatsu, M. *et al.* Impairment of starvation-induced and constitutive autophagy in *Atg7*-deficient mice. *J. Cell Biol.* **169**, 425–434 (2005).
- Betz, U. A., Vosshehrich, C. A., Rajewsky, K. & Muller, W. Bypass of lethality with mosaic mice generated by *Cre-loxP*-mediated recombination. *Curr. Biol.* **6**, 1307–1316 (1996).
- Mizushima, N. *et al.* Dissection of autophagosome formation using Apg5-deficient mouse embryonic stem cells. *J. Cell Biol.* **152**, 657–667 (2001).
- Kabeya, Y. *et al.* LC3, a mammalian homologue of yeast Apg8p, is localized in autophagosome membranes after processing. *EMBO J.* **19**, 5720–5728 (2000).
- Cote, F., Collard, J. F. & Julien, J. P. Progressive neuropathy in transgenic mice expressing the human neurofilament heavy gene: a mouse model of amyotrophic lateral sclerosis. *Cell* **73**, 35–46 (1993).
- Mangiarini, L. *et al.* Exon 1 of the *HD* gene with an expanded CAG repeat is sufficient to cause a progressive neurological phenotype in transgenic mice. *Cell* **87**, 493–506 (1996).
- Kikuchi, T., Mukoyama, M., Yamazaki, K. & Moriya, H. Axonal degeneration of ascending sensory neurons in gracile axonal dystrophy mutant mouse. *Acta Neuropathol. (Berl.)* **80**, 145–151 (1990).
- Sotelo, C. Axonal abnormalities in cerebellar Purkinje cells of the 'hyperspiny Purkinje cell' mutant mouse. *J. Neurocytol.* **19**, 737–755 (1990).
- Lossi, L., Mioletti, S. & Merighi, A. Synapse-independent and synapse-dependent apoptosis of cerebellar granule cells in postnatal rabbits occur at two subsequent but partly overlapping developmental stages. *Neuroscience* **112**, 509–523 (2002).
- Sakai, K. & Miyazaki, J. A transgenic mouse line that retains Cre recombinase activity in mature oocytes irrespective of the cre transgene transmission. *Biochem. Biophys. Res. Commun.* **237**, 318–324 (1997).
- Kuhn, R., Schwenk, F., Aguet, M. & Rajewsky, K. Inducible gene targeting in mice. *Science* **269**, 1427–1429 (1995).
- Kopito, R. R. Aggregates, inclusion bodies and protein aggregation. *Trends Cell Biol.* **10**, 524–530 (2000).
- Saudou, F., Finkbeiner, S., Devys, D. & Greenberg, M. E. Huntingtin acts in the nucleus to induce apoptosis but death does not correlate with the formation of intranuclear inclusions. *Cell* **95**, 55–66 (1998).
- Kuemmerle, S. *et al.* Huntington aggregates may not predict neuronal death in Huntington's disease. *Ann. Neurol.* **46**, 842–849 (1999).
- Taylor, J. P. *et al.* Aggregates protect cells by enhancing the degradation of toxic polyglutamine-containing protein. *Hum. Mol. Genet.* **12**, 749–757 (2003).
- Arrasate, M., Mitra, S., Schweitzer, E. S., Segal, M. R. & Finkbeiner, S. Inclusion body formation reduces levels of mutant huntingtin and the risk of neuronal death. *Nature* **431**, 805–810 (2004).
- Tanaka, M. *et al.* Aggregates formed by α -synuclein and synphilin-1 are cytoprotective. *J. Biol. Chem.* **279**, 4625–4631 (2004).
- Bjorkoy, G. *et al.* p62/SQSTM1 forms protein aggregates degraded by autophagy and has a protective effect on huntingtin-induced cell death. *J. Cell Biol.* **171**, 603–614 (2005).
- Mori, H. *et al.* Socs3 deficiency in the brain elevates leptin sensitivity and confers resistance to diet-induced obesity. *Nature Med.* **10**, 739–743 (2004).
- Yamamoto, A. *et al.* Stacks of flattened smooth endoplasmic reticulum highly enriched in inositol 1,4,5-trisphosphate (InsP₃) receptor in mouse cerebellar Purkinje cells. *Cell Struct. Funct.* **16**, 419–432 (1991).

Supplementary Information is linked to the online version of the paper at www.nature.com/nature. A summary figure is also included.

Acknowledgements We thank H. Neko, M. Miwa and Y. Kabeya for technical assistance. We also thank J. Miyazaki for the donation of CAG-Cre transgenic mice, T. Yoshimori for the anti-LC3 antibody, E. Yamada for histological examination, M. Yuzaki for the rotarod analysis, and A. Kuma for discussion. We thank Z. Yue for critical reading of the manuscript. This work was supported in part by Grants-in-Aid for Scientific Research from the Ministry of Education, Culture, Sports, Science and Technology of Japan. The authors thank the Yamada Science Foundation and the Cell Science Research Foundation for their financial support.

Author Contributions T.H. performed most of the experiments to characterize the neuron-specific knockout mice. M.M. analysed *Atg5*^{-/-} mice. K.N., Y.N., R.S.-M. and M.Y. generated *Atg5*^{lox} chimaeric mice. A.Y. performed electron microscopy. K.M. and I.S. performed histological analysis. H.O. provided nestin-Cre mice and participated in manuscript preparation. N.M. conceived the experiments and generated the targeting vector. T.H. and N.M. wrote the paper.

Author Information Reprints and permissions information is available at ngp.nature.com/reprintsandpermissions. The authors declare no competing financial interests. Correspondence and requests for materials should be addressed to N.M. (nmizu@rinshoken.or.jp).